IEEE Access
Multidisciplinary | Rapid Review | Open Access Journal

Received December 1, 2020, accepted December 23, 2020, date of publication December 28, 2020, date of current version January 7, 2021.

*Digital Object Identifier 10.1109/ACCESS.2020.3047686*

# 2D DOA Estimation Exploiting Vertical Synthetic Planar Arrays

**GUIYU WANG, ZESONG FEI, (Senior Member, IEEE), AND SHIWEI REN**
School of Information and Electronics, Beijing Institute of Technology, Beijing 100081, China

Corresponding author: Shiwei Ren (renshiwei@bit.edu.cn)

This work was supported in part by the National Natural Science Foundation of China under Grant 61801024.

**ABSTRACT** In this paper, vertical motions of sparse linear arrays (SLAs) are utilized to generate equivalent synthetic planar arrays for two-dimensional (2D) direction-of-arrival (DOA) estimation. The proposed array geometry named vertical synthetic planar array (VSPA) consists of an arbitrary SLA on the x-axis and a series of its time-shifted arrays in the vertical orientation. With the original linear array and the moving trail known, the difference coarray of VSPA can be easily obtained. By utilizing both the synthetic aperture processing and the coarray technique, VSPA has the ability to construct a synthetic planar array with only an SLA used. Compared with the traditional sparse planar arrays (SPAs), such as 2D nested array and 2D coprime array, VSPA can achieve higher degree-of-freedom and improved 2D DOA estimation performance with the same number of sensors. Moreover, as different original linear arrays and moving trails can be chosen for different applications, the construction of VSPA is of high flexibility. Numerical simulations are presented to verify the superiority of the proposed VSPA geometry over other typical SPAs.

**INDEX TERMS** Difference coarray, DOA estimation, sparse planar array, synthetic aperture, vertical motion.

## I. INTRODUCTION

Direction-of-arrival (DOA) estimation has been playing a significant role in array signal processing for various applications, such as radar, sonar, communication and satellite navigation [1]–[4]. Compared with uniform arrays, sparse arrays can detect more sources and reach higher degree-of-freedom (DOF) by using the coarray technique [5].

In the previous works, several coarray-based sparse linear arrays (SLAs) are proposed to increase the virtual DOF and obtain better DOA estimation performance. The minimum redundancy arrays (MRAs) [6] and minimum hole arrays (MHAs) [7] are proposed to minimize the redundant virtual sensors and the holes in the difference coarray (DcA). However, both of them suffer from the absence of closed-form expressions and the need of exhaustive searching. Recently, nested arrays (NAs) [8] and coprime arrays (CAs) [9] have attracted much attention for their superiority in DOF enhancement. By using $\mathcal{O}(N)$ physical sensors, $\mathcal{O}(N^2)$ impinging sources can be detected with the covariance matrix of the received signals considered. Based on the coarray concept, some more effective SLAs were developed to further enhance the DOF or reduce the mutual coupling effects. These SLAs include super nested arrays (SNAs) [10], [11], augmented nested arrays (ANAs) [12], generalized coprime arrays [13], and NAs/CAs with difference-sum coarray [14], [15].

Note that the above SLAs are placed in a stationary environment with sensors fixed. Recent works have shown that array motions make it possible to further increase the DOF by utilizing the synthetic aperture (SA) processing technique [16]–[18]. Array motions are usually realized by mounting arrays to a moving platform which can be air-borne, vehicle-attached or ship-based. In [19], SA processing is applied to CAs with coprime integers $M, N$. By moving $N/2(N > M)$ half wavelengths, the CA along with its shifted array can generate a hole-free DcA. However, the stationary of the signal environment is hard to be guaranteed over such a long time period. Thus in [20], a short translation motion of the array (merely one half wavelength) is assumed so that the environment can be considered unchanged. And then the inter-sensor spacing of NAs is expanded $r$ times to construct the dilated nested arrays (DNAs). It is shown that the DNAs can provide a hole-free DcA with such short motion. Furthermore, the authors analyze the DOA estimation performance of other moving SLAs, such as CAs, NAs, MRAs, MHAs

The associate editor coordinating the review of this manuscript and approving it for publication was Mohammad Zia Ur Rahman.

and sparse ULAs (SULAs), with the same short translation assumption [21]. Recently, based on the fact that longer synthetic distance can be realized when the signal environment changes sufficiently slowly [22], the multi-level DNA is proposed to futher increase the array DOF by moving the array $K$ times [23]. Besides, [24] provides the maximum moving time at a slow moving speed to hold the signal environment stationary. Consequently, the final DOF of the synthetic array can be tripled without increasing the inter-sensor spacing as DNAs do. Moreover, the possible errors brought in by the array motion in the presence of phase noise have also been taken into consideration [25]. Although motions of different SLAs along the direction of the array layout have been discussed and analyzed, array motions along the vertical direction are still rarely mentioned.

In this paper, we provide the geometry of the vertical synthetic planar array (VSPA) for two-dimensional (2D) DOA estimation. By moving an one-dimensional (1D) linear array on the x-axis vertically along the y-axis direction, a synthetic planar array is formed by the original linear array and a series of its time-shifted arrays. By combining all the received data of each measurement during the motion, the equivalent signal model can be established through the SA processing. Besides, in order to increase the DOF for better DOA estimation performance, the coarray technique is applied to generate the DcA. Properties of the DcA of VSPA are then provided. Moreover, the closed-form expressions of the holes and sensor positions of different VSPA-based structures, such as CA, NA and MRA, are provided. The main advantages of the VSPA geometry include the high virtual DOF with small sensor number, and the flexibility in array design. Simulations verify that the VSPA-based structures can detect more sources and reach higher performance in 2D DOA estimation with the same number of physical sensors as typical sparse planar arrays (SPAs). The main contributions of our work are listed as follows.

1) We derive the method of VSPA construction, which utilizes the array vertical motions to construct a synthetic planar array with merely a linear array.
2) The proposed VSPA structure can achieve dramatically high uniform DOF with only a few physical sensors and the concept of difference coarray.
3) The structure of a VSPA is of very high flexibility in design with different combinations of the original linear arrays and the moving trails.

The remainder of this paper is organized as follows. The basic structure of some typical SPAs and the concept of DcA are reviewed in Section II. In Section III, the signal model of the VSPAs and synthetic aperture processing are summarized, and the computational complexity is analyzed. Next, some main properties of the DcA of VSPAs are disscussed in Section IV. The closed-form expressions of DcAs of several VSPA-based structures as well as the performance analysis of them are then presented. In Section V, the number of detectable sources of some typical SPAs and VSPA-based structures are given. Then, the performance of 2D DOA estimation are evaluated with the same number of physical sensors, demonstrating the superiority of the proposed VSPA geometry. Section VI concludes the paper.

*Notations:* We use lower-case (upper-case) boldface symbols to represent vectors (matrices). $(\cdot)^T$ implies the transpose, whereas $(\cdot)^*$ and $(\cdot)^H$ denotes complex conjugation and complex conjugate transpose of a matrix or vector, respectively. $vec(\cdot)$ denotes the vectorization operator that turns a matrix into a vector. $diag(\mathbf{x})$ denotes a diagonal matrix with the elements of $\mathbf{x}$ as the diagonal elements. $tr(\cdot)$ denotes the trace of a matrix. $\otimes$ implies the Kronecker product and $\odot$ implies the Khatri-Rao (KR) product. $\lfloor a \rfloor$ rounds $a$ to the nearest integer no more than $a$, while $\lceil a \rceil$ rounds $a$ to the nearest integer no less than $a$.

## II. REVIEW OF SPAs AND COARRAY

In this section, the concept of DcA is given first. Then brief review of two most commonly used SPAs, namely the 2D nested array (2D-NA) [26], [27] and 2D coprime array (2D-CA) [28], [29], as well as their corrsponding DcAs are provided.

*Definition 1 (Difference Coarray):* For an array whose sensor positions are specified by set $\mathbb{S}$, the DcA is defined as the set of differences between every two sensor positions in $\mathbb{S}$, i.e.,

$$\mathbb{D} = \{\mathbf{p}_1 - \mathbf{p}_2 \,|\, \mathbf{p}_1, \mathbf{p}_2 \in \mathbb{S}\}. \tag{1}$$

■

Note that for some SPAs, their DcAs are not completely consecutive. Generally, the largest uniform rectangular array (URA) in the DcA is extracted to execute the subspace-based DOA estimation methods. For the sake of evaluating the performance of arrays, the definitions of array virtual aperture as well as DOF are given as follows:

*Definition 2 (Array Virtual Aperture):* For a planar array $\mathbb{S}$ with an rectangular DcA $\mathbb{D}$, suppose $\mathbf{p}_1 = (x_1, y_1)$ and $\mathbf{p}_2 = (x_2, y_2)$ are two furthest virtual sensors in $\mathbb{D}$. Then, the array virtual aperture (AVP) is the product of the absolute differences in two coordinates between $\mathbf{p}_1$ and $\mathbf{p}_2$, denoted as $\mathcal{A} = |x_1 - x_2| \times |y_1 - y_2|$. ■

*Definition 3 (Degree-of-Freedom):* For an array $\mathbb{S}$, let $\mathbb{D}$ denote the corresponding DcA, and $\mathbb{U}$ denote the largest URA area available for DOA estimation in $\mathbb{D}$. Then, the cardinalities of $\mathbb{D}$ and $\mathbb{U}$ are respectively called DOF and uniform DOF (uDOF), denoted as $\mathcal{D}$ and $\mathcal{U}$. ■

A 2D-NA consists of a dense uniform array and a sparse uniform array which share the first sensor at the origin. The dense array is of $N_1 \times N_1$ sensors with the inter-sensor spacing of $d = \frac{\lambda}{2}$, where $\lambda$ denotes the wavelength. And the sparse array is of $N_2 \times N_3$ sensors with the inter-sensor spacing of $N_1 d$. The total number of sensors is $N_s = N_1^2 + N_2 N_3 - 1$. For simplicity, the unit inter-sensor spacing $d$ is omitted in the rest of this paper. The sensor positions of 2D-NA are given by

$$\begin{aligned}\mathbb{S}_{\text{2D-NA}} = &\{(x, y) \,|\, x, y \in [0 : 1 : (N_1 - 1)]\} \\ &\cup \{(x, y) \,|\, x \in [0 : N_1 : (N_2 - 1)N_1], \\ &\quad y \in [0 : N_1 : (N_3 - 1)N_1]\},\end{aligned} \tag{2}$$

where $[a : s : b]$ represents the values in the range of $[a, b]$ sampled by step $s$. The corresponding AVP and uDOF of 2D-NA are

$$\begin{aligned}\mathcal{A}_{\text{2D-NA}} &= 2N_1(N_2-1)\times 2N_1(N_3-1),\\ \mathcal{U}_{\text{2D-NA}} &= N_1N_2\times N_1N_3.\end{aligned} \tag{3}$$

Notice that the uDOF is much lower than the AVP because of the existence of holes in the DcA. Only the virtual sensors in the largest URA within DcA can be used in the 2D DOA estimation.

An example of 2D-NA is depicted in Fig. 1, where $N_1 = 3$, $N_2 = N_3 = 4$, and the number of sensors is totally $N_s = 24$. It can be seen from Fig. 1(b) that the DcA of 2D-NA contains two URAs of the same size, which are marked out by the dashline. The AVP and uDOF are $\mathcal{A}_{\text{2D-NA}} = 18 \times 18$ and $\mathcal{U}_{\text{2D-NA}} = 12 \times 12$, respectively. One of the URA is in the area of $\mathbb{U}_{\text{2D-NA}} = \{(x, y)\,|\,x, y \in [-2 : 1 : 9]\}$. The other is symmetric about the origin. Since only one of the two URAs can be fully used, the performance of 2D DOA estimation is limited.

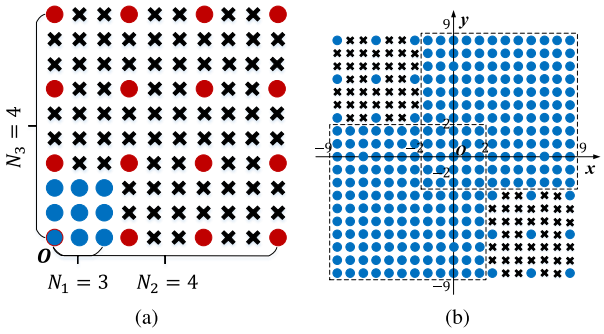


**FIGURE 1.** Example of a 2D-NA with $N_1 = 3, N_2 = N_3 = 4$. (a) The physical array. (b) The DcA. The blue and red bullets denote sensors in the two subarrays, and the black crosses denote positions without sensors.

A 2D-CA consists of two uniform subarrays with the first sensors overlapped. One subarray has $N \times N$ sensors with inter-sensors spacing of $Md$. The other one has $M \times M$ sensors with inter-sensor spacing of $Nd$. $M$ and $N$ are coprime integers. The total number of sensors is $N_s = M^2 + N^2 - 1$. Without loss of generality, we assume $M < N$. Then, the sensor positions of 2D-CA are given by

$$\begin{aligned}\mathbb{S}_{\text{2D-CA}} = &\{(x, y)\,|\,x, y \in [0 : M : (N-1)M]\}\\ &\cup\{(x, y)\,|\,x, y \in [0 : N : (M-1)N]\}.\end{aligned} \tag{4}$$

The corresponding AVP and uDOF of 2D-CA are

$$\begin{aligned}\mathcal{A}_{\text{2D-CA}} &= 2M(N-1)\times 2M(N-1),\\ \mathcal{U}_{\text{2D-CA}} &= (2M+N-1)\times(2M+N-1).\end{aligned} \tag{5}$$

Fig. 2 shows an example of 2D-CA for $M = 3, N = 4$. The total number of sensors is $N_s = 24$. The URAs in DcA locate in $\mathbb{U}_{\text{2D-CA}} = \{(x, y)\,|\,x \in [-6 : 1 : 2], y \in [-2 : 1 : 6]\}$ and the mirrored area, as shown in Fig. 2(b). The corresponding AVP and uDOF are $\mathcal{A}_{\text{2D-CA}} = 18 \times 18$ and $\mathcal{U}_{\text{2D-CA}} = 9 \times 9$, respectively. Although the sensor number and AVP are the same as that of the above example of 2D-NA, the uDOF of 2D-CA is lower, which leads to worse 2D DOA estimation performance.

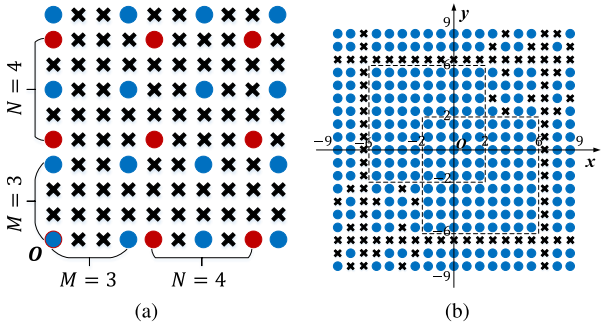


**FIGURE 2.** Example of a 2D-CA with $M = 3, N = 4$. (a) The physical array. (b) The DcA.

## III. THE PROPOSED METHOD

### A. THE DERIVATION OF VSPA

Consider a linear array with $N_s$ sensors placed horizontally (on the x-axis) moving at a constant velocity $v_y$ vertically (along the y-axis). Let $\mathfrak{p}_o = [p_1, p_2, \ldots, p_{N_s}]$ denote the 1D sensor positions of the original linear array, and the first sensor is assumed as the reference, i.e., $p_1 = 0$. Then the array sensors are positioned at $\mathbb{S}_1 = \{(x, 0)\,|\,x \in \mathfrak{p}_o\}$. Let $\tau$ denote the unit time interval for the array to move a distance of $d$, i.e., $v_y\tau = d$. Assume totally $M_s$ measurements are taken when the array moves vertically and arrives at positions $\{(x, l_i)\,|\,x \in \mathfrak{p}_o, i = 1, 2, \ldots, M_s\}$, then the set $\mathfrak{p}_m = \{l_1, l_2, \ldots, l_{M_s}\}$ is called the *moving trail*. The schematic is illustrated in Fig. 3 where a nested array is taken as an example. The solid blue circles and dotted red circles represent the sensor positions of the original and the shifted arrays, respectively.

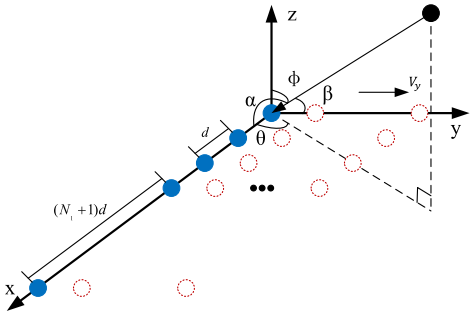


**FIGURE 3.** The schematic diagram of a vertically moving linear array.

Suppose that the received signals are from $Q$ far-field uncorrelated narrowband sources, which are described as $s_q(t), t = T_s, 2T_s, \ldots, K_sT_s$, for $q = 1, 2, \ldots, Q$, where $T_s$ and $K_s$ represent the sampling interval and the number of snapshots respectively. The power of the $q$th source is $\sigma_q^2$. The arrival azimuth angle and elevation angle of the $q$th source are denoted as $\theta_q \in [0, 2\pi]$ and $\phi_q \in [0, \frac{\pi}{2}]$

respectively. Define $\cos(\alpha_q)=\cos(\theta_q)\sin(\phi_q)$ and $\cos(\beta_q)=\sin(\theta_q)\sin(\phi_q)$. Then, the output of the receive array at moment $t$ is expressed as

$$\begin{aligned}\mathbf{x}(t) &= \sum_{q=1}^{Q} s_q(t)\exp\left(-j2\pi\frac{v_y t}{\lambda}\cos(\beta_q)\right)\mathbf{a}_q+\mathbf{n}(t)\\ &= \mathbf{A}\mathbf{s}(t)+\mathbf{n}(t),\end{aligned} \tag{6}$$

where

$$\begin{aligned}\mathbf{a}_q = \Big[&1,\exp(-j2\pi\frac{d}{\lambda}(x_2\cos(\alpha_q)+y_2\cos(\beta_q))),\\ &\ldots,\exp(-j2\pi\frac{d}{\lambda}(x_{N_s}\cos(\alpha_q)+y_{N_s}\cos(\beta_q)))\Big]^T\end{aligned} \tag{7}$$

is the steering vector and

$$\begin{aligned}\mathbf{s}(t) = \big[&s_1(t)\exp(-j2\pi v_y t\cos(\beta_1)/\lambda),\\ &s_2(t)\exp(-j2\pi v_y t\cos(\beta_2)/\lambda)\\ &,\ldots,\ s_Q(t)\exp(-j2\pi v_y t\cos(\beta_Q)/\lambda)\big]^T\end{aligned} \tag{8}$$

is the signal vector. $\mathbf{A}=[\mathbf{a}_1,\mathbf{a}_2,\ldots,\mathbf{a}_Q]\in\mathbb{C}^{N_s\times Q}$ denotes the array manifold matrix, and $\mathbf{n}(t)$ is the zero-mean complex additive white Gaussian noise vector with power $\sigma_n^2$.

Similarly, at moment $t+l_i\tau$, the received signal changes into

$$\begin{aligned}\mathbf{x}(t+l_i\tau) &= \sum_{q=1}^{Q} s_q(t+l_i\tau)\exp(-j2\pi\frac{v_y t}{\lambda}\cos(\beta_q))\\ &\quad\cdot\exp(-j2\pi\frac{v_y l_i\tau}{\lambda}\cos(\beta_q))\mathbf{a}_q+\mathbf{n}(t+l_i\tau)\\ &= \mathbf{B}_i\bar{\mathbf{s}}(t+l_i\tau)+\mathbf{n}(t+l_i\tau),\end{aligned} \tag{9}$$

where $\mathbf{B}_i=[\mathbf{b}_{i,1},\mathbf{b}_{i,2},\ldots,\mathbf{b}_{i,Q}]\in\mathbb{C}^{N_s\times Q}$, $\mathbf{B}_1=\mathbf{A}$ with

$$\begin{aligned}\mathbf{b}_{i,q} &= \exp(-j2\pi\frac{v_y l_i\tau\cos(\beta_q)}{\lambda})\mathbf{a}_q\\ &= \big[\exp(-j\pi l_i\cos(\beta_q)),\\ &\quad\exp(-j\pi(x_2\cos(\alpha_q)+(y_2+l_i)\cos(\beta_q))),\ldots,\\ &\quad\exp(-j\pi(x_{N_s}\cos(\alpha_q)+(y_{N_s}+l_i)\cos(\beta_q)))\big]^T,\end{aligned} \tag{10}$$

and

$$\begin{aligned}\bar{\mathbf{s}}(t+l_i\tau) = \big[&s_1(t+l_i\tau)\exp(-j2\pi v_y t\cos(\beta_1)/\lambda),\\ &s_2(t+l_i\tau)\exp(-j2\pi v_y t\cos(\beta_2)/\lambda),\ldots,\\ &s_Q(t+l_i\tau)\exp(-j2\pi v_y t\cos(\beta_Q)/\lambda)\big]^T.\end{aligned} \tag{11}$$

As we have assumed that the signals are narrowband with carrier frequency $f_c$, $s_q(t+l_i\tau)=\exp(j2\pi f_c l_i\tau)s_q(t)$ holds. Thus, (9) can be rewritten as

$$\mathbf{x}(t+l_i\tau)=\exp(j2\pi f_c l_i\tau)\mathbf{B}_i\mathbf{s}(t)+\mathbf{n}(t+l_i\tau). \tag{12}$$

By utilizing the following phase correction technique [30] with the factor $\exp(-j2\pi f_c l_i\tau)$, we can obtain the phase synchronized received signal vector as

$$\begin{aligned}\tilde{\mathbf{x}}(t+l_i\tau) &= \mathbf{x}(t+l_i\tau)\exp(-j2\pi f_c l_i\tau)\\ &= \mathbf{B}_i\mathbf{s}(t)+\tilde{\mathbf{n}}(t+l_i\tau),\end{aligned} \tag{13}$$

where $\tilde{\mathbf{n}}(t+l_i\tau)=\exp(-j2\pi f_c l_i\tau)\mathbf{n}(t+l_i\tau)$. Note that during the entire period of motion, since the signals are from far-field sources, the signal environment and source directions with respect to the array are assumed to be unchanged.

Stacking all the signals received in each measurement into a single vector yields

$$\begin{aligned}\mathbf{y}(t) &= \begin{bmatrix}\mathbf{x}(t)\\ \tilde{\mathbf{x}}(t+l_2\tau)\\ \vdots\\ \tilde{\mathbf{x}}(t+l_i\tau)\\ \vdots\\ \tilde{\mathbf{x}}(t+l_{M_s}\tau)\end{bmatrix} = \begin{bmatrix}\mathbf{A}\mathbf{s}(t)+\mathbf{n}(t)\\ \mathbf{B}_2\mathbf{s}(t)+\tilde{\mathbf{n}}(t+l_2\tau)\\ \vdots\\ \mathbf{B}_i\mathbf{s}(t)+\tilde{\mathbf{n}}(t+l_i\tau)\\ \vdots\\ \mathbf{B}_{M_s}\mathbf{s}(t)+\tilde{\mathbf{n}}(t+l_{M_s}\tau)\end{bmatrix}\\ &= \mathbf{C}\mathbf{s}(t)+\hat{\mathbf{n}}(t),\end{aligned} \tag{14}$$

where

$$\mathbf{C}=\left[\mathbf{A}^T,\mathbf{B}_2^T,\ldots,\mathbf{B}_{M_s}^T\right]^T=[\mathbf{c}_1,\mathbf{c}_2,\ldots,\mathbf{c}_Q]$$

and

$$\hat{\mathbf{n}}(t)=[\mathbf{n}^T(t),\tilde{\mathbf{n}}^T(t+l_2\tau),\ldots,\tilde{\mathbf{n}}^T(t+l_{M_s}\tau)]^T.$$

$\mathbf{y}(t)$ can be equivalently treated as the data received by a synthetic planar array at the moment $t$. This kind of synthetic planar array constructed upon moving a specific linear array in a specific trail vertically is named as VSPA. Due to the assupmtion that the sources and noise are uncorrelated, the covariance matrix of $\mathbf{y}(t)$ can be expressed as

$$\mathbf{R}_y=E[\mathbf{y}(t)\mathbf{y}^H(t)]=\mathbf{C}\mathbf{R}_s\mathbf{C}^H+\sigma_n^2\mathbf{I}_{N_{\mathrm{SA}}}, \tag{15}$$

where $E(\cdot)$ is the statistical expectation operator, $\mathbf{R}_s=E[\mathbf{s}(t)\mathbf{s}^H(t)]=diag([\sigma_1^2,\sigma_2^2,\ldots,\sigma_Q^2])$ is the source covariance matrix, and $\mathbf{I}_{N_{\mathrm{SA}}}$ is an identity matrix with $N_{\mathrm{SA}}$ being the total number of sensors in VSPA. In practice, since the true statistics of $\mathbf{R}_y$ is unavailable, it is usually estimated from the $K_s$ snapshots by $\hat{\mathbf{R}}_y=\frac{1}{K_s}\sum_{k=1}^{K_s}\mathbf{y}(t)\mathbf{y}^H(t)$.

Vectorizing $\mathbf{R}_y$ yields

$$\mathbf{z}=vec(\mathbf{R}_y)=(\mathbf{C}^*\odot\mathbf{C})\tilde{\mathbf{p}}+\sigma_n^2\mathbf{i}, \tag{16}$$

where the $q$th column of $\mathbf{C}^*\odot\mathbf{C}$ is $\mathbf{c}_q^*\otimes\mathbf{c}_q$, $\tilde{\mathbf{p}}=[\sigma_1^2,\sigma_2^2,\ldots,\sigma_Q^2]^T$, and $\mathbf{i}=vec(\mathbf{I}_{N_{\mathrm{SA}}})$. By extracting all the consecutive unique elements of the DcA from $\mathbf{z}$ and applying the 2D spatial smoothing technique [31], the full rank matrix $\mathbf{R}_z$ can be constructed. Then, the subspace-based 2D DOA estimation methods can be executed to $\mathbf{R}_z$. In this paper, we utilize the 2D unitary ESPRIT algorithm [32].

### B. COMPUTATIONAL COMPLEXITY ANALYSIS

In the following, we will analyze the computational complexity of our proposed method. Note that only the real multiplications in the method are taken into account. The additions and other low-complexity operations are ignored. The computations mainly appear in the following three stages.

1) The covariance matrix $\mathbf{R}_y$. Since $\mathbf{y}(t)$ is a $N_sM_s\times 1$ vector of VSPA, $\mathbf{R}_y$ need $N_s^2M_s^2$ multiplications for

each snapshot. Therefore, for all $K_s$ snapshots, there are totally $N_s^2 M_s^2 K_s$ multiplications.

2) The 2D spatial smoothing. Vectorizing $\mathbf{R}_y$ yields the $N_s^2 M_s^2 \times 1$ vector $\mathbf{z}$. Suppose that the uDOF of VSPA is $\mathcal{U} = L_{ux} \times L_{uy}$. Thus, the equivalent single snapshot data vector of the central URA extrated from the unrepeated elements of $\mathbf{z}$ is $\mathbf{z}_u \in \mathbb{C}^{L_{ux}L_{uy}\times 1}$. Denote $\widetilde{L}_x = \frac{L_{ux}+1}{2}$ and $\widetilde{L}_y = \frac{L_{uy}+1}{2}$. After spatial smoothing, an $\widetilde{L}_x\widetilde{L}_y \times \widetilde{L}_x\widetilde{L}_y$ covariance matrix $\mathbf{R}_z$ with full-rank can be obtained. This process needs $\mathcal{O}(\widetilde{L}_x^3\widetilde{L}_y^3)$ multiplications.

3) The 2D Unitary ESPRIT algorithm. Finally, based on $\mathbf{R}_z$ we conduct 2D Unitary ESPRIT algorithm for 2D DOA estimation. According to [33], during the algorithm about $\mathcal{O}((\widetilde{L}_x\widetilde{L}_y)^3 + \widetilde{L}_x^3 + \widetilde{L}_y^3 + (\widetilde{L}_x\widetilde{L}_y)^2 Q + \widetilde{L}_x\widetilde{L}_y Q^2 + Q^3)$ real multiplications are needed.

As a result, the total computational complexity of our proposed method is the sum of the above three parts. Notice the fact that $\mathcal{O}(\widetilde{L}_x\widetilde{L}_y) \approx \mathcal{O}(N_s^2 M_s^2)$ and $Q \ll \widetilde{L}_x\widetilde{L}_y$. Thus, when the number of snapshots $K_s$ is infinite, the complexity is approximate to $\mathcal{O}(\widetilde{L}_x^3\widetilde{L}_y^3)$.

## IV. DIFFERENCE COARRAY OF VSPA

As described in Section III-A, a VSPA is the equivalent synthetic planar array of an arbitrary linear array moving in vertical trail. The sensor positions of the linear array in the $i$th measurement are expressed as

$$\mathbb{S}_i = \{(x, l_i) \,|\, x \in \mathfrak{p}_o, l_i \in \mathfrak{p}_m\}. \tag{17}$$

Combining the sensor positions of the original linear array and all the shifted arrays, the entire set of sensor positions of VSPA is expressed as

$$\mathbb{S}_{\text{VSPA}} = \mathbb{S}_1 \cup \mathbb{S}_2 \cup \ldots \cup \mathbb{S}_{M_s}. \tag{18}$$

Thus, the DcA of VSPA has the form of

$$\mathbb{D}_{\text{VSPA}} = \bigcup_{i,j=1}^{M_s} \mathbb{S}_i - \mathbb{S}_j. \tag{19}$$

The following properties hold for the DcA of VSPA.

*Proposition 1 (Consecutive Area in DcA):* Let $\mathbb{D}_{\mathfrak{p}_o} = \mathfrak{p}_o - \mathfrak{p}_o$ and $\mathbb{D}_{\mathfrak{p}_m} = \mathfrak{p}_m - \mathfrak{p}_m$ denote the 1D DcAs of the original linear array and the moving trail, respectively. Moreover, $\mathcal{A}_{\mathfrak{p}_o}$, $\mathcal{A}_{\mathfrak{p}_m}$, $\mathcal{U}_{\mathfrak{p}_o}$ and $\mathcal{U}_{\mathfrak{p}_m}$ are the corresponding AVPs and uDOF. Then, the relationships among the DcAs of $\mathbb{S}_{\text{VSPA}}$, $\mathfrak{p}_o$ and $\mathfrak{p}_m$ can be concluded as follows.

1) Each row and column of $\mathbb{D}_{\text{VSPA}}$ have the same geometries as $\mathbb{D}_{\mathfrak{p}_o}$, and $\mathbb{D}_{\mathfrak{p}_m}$, respectively, i.e., $\mathbb{D}_{\text{VSPA}} = \{(x, y) \,|\, x \in \mathbb{D}_{\mathfrak{p}_o}, y \in \mathbb{D}_{\mathfrak{p}_m}\}$.
2) Subsequently, the largest URA in the DcA is formed by both the largest ULA parts in the DcA of the original linear array and the moving trail, i.e., $\mathbb{U}_{\text{VSPA}} = \{(x, y) \,|\, x \in \mathbb{U}_{\mathfrak{p}_o}, y \in \mathbb{U}_{\mathfrak{p}_m}\}$.
3) Finally, the AVP of VSPA is $\mathcal{A}_{\text{VSPA}} = \mathcal{A}_{\mathfrak{p}_o} \times \mathcal{A}_{\mathfrak{p}_m}$, and the corresponding uDOF is $\mathcal{U}_{\text{VSPA}} = \mathcal{U}_{\mathfrak{p}_o} \times \mathcal{U}_{\mathfrak{p}_m}$.

■

As each row and each column of VSPA are respectively identical, the above properties can be easily proved by the geometric relations. Next, we take some examples to help illustrate the characteristics of VSPA. Note that we name a certain VSPA structure in the form of "*VSPA-origin-trail*". The middle affix *origin* represents the structure of the original linear array, and the suffix *trail* represents the structure of the moving trail.

### A. VSPA-CA-CA

A VSPA-CA-CA derives from a CA with $N_s = M+N-1$ sensors moving in the trail of another CA. For simplicity, we let the trail have the identical geometry with the original CA. Note that the geometry of VSPA-CA-CA is different from the 2D-CA. Each row and column of the VSPA-CA-CA is a CA, while the 2D-CA is formed by two uniform planar subarrays with only the first row and the first column being CAs. It is known that the DcA of CA has holes. We can directly obtain the positions of holes in the DcA of VSPA-CA-CA expressed as [14]

$$\mathbb{H}_{\text{VSPA-CA-CA}} = \{(x, y) \,|\, x, y = \pm(aM + bN), a \geq 0, b > 0, \\ 0 < aM + bN < M(N-1)\}. \tag{20}$$

The corresponding AVP and uDOF of VSPA-CA-CA are

$$\begin{aligned} \mathcal{A}_{\text{2D-CA}} &= 2M(N-1) \times 2M(N-1), \\ \mathcal{U}_{\text{VSPA-CA-CA}} &= (2M + 2N - 1) \times (2M + 2N - 1). \end{aligned} \tag{21}$$

The AVP of VSPA-CA-CA is the same as that of the 2D-CA while the uDOF of VSPA-CA-CA is higher than that of 2D-CA. As a result, the VSPA-CA-CA uses only $N_s = M+N-1$ physical sensors to reach $\mathcal{O}(4M^2N^2)$ uDOF. Another advantage of this structure comes from the sparse distribution of CA which brings less mutual coupling effect. However, the holes still limit the uDOF as well as the number of detectable sources.

Note that we always aim at maximizing the final uDOF. Therefore, the optimum values of coprime integers $M, N$ are selected as close as possible.

Fig. 4 shows a VSPA-CA-CA with $M = 3, N = 4$, which are selected properly to obtain the optimum uDOF. The total number of physical sensors is $N_s = 6$. Fig. 4(a) shows the physical geometry where the solid blue circles denote the original CA and the dashed red circles denote the moving trail. Fig. 4(b) draws the cooresponding DcA. In this case, the AVP is $\mathcal{A}_{\text{VSPA-CA-CA}} = 18 \times 18$ and the uDOF is $\mathcal{U}_{\text{VSPA-CA-CA}} = 13 \times 13$. Compared with the 2D-CA in Fig. 2, the VSPA-CA-CA can obtain the same AVP but higher uDOF with fewer physical sensors.

### B. VSPA-NA-NA

Similarly, a VSPA-NA-NA comes from an 1D NA moving along the trail of 1D NA vertically. Thus, each row and column of VSPA-NA-NA is an NA, whereas neither of the rows or columns in 2D-NA is of NA structure. Note that in this paper we only consider the case of two-level NA since its DcA

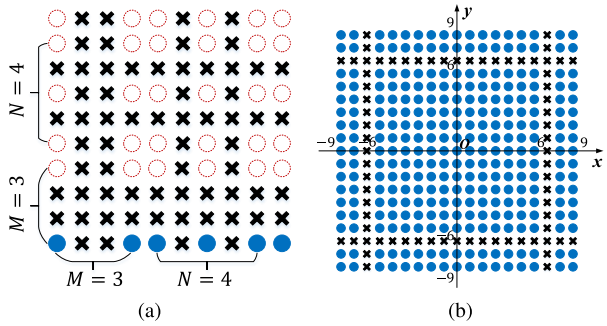


**FIGURE 4.** The VSPA-CA-CA for $M = 3, N = 4$. (a) The synthetic array. (b) The DcA.

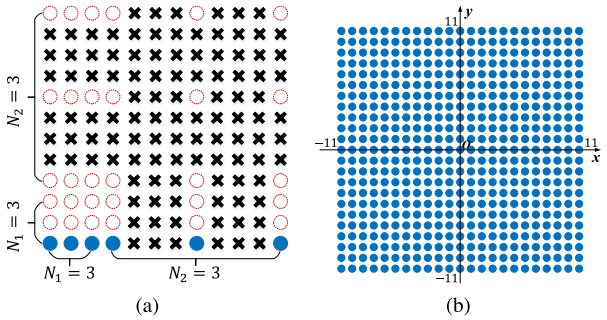


**FIGURE 5.** The VSPA-NA-NA for $N_1 = N_2 = 3$. (a) The synthetic array. (b) The DcA.

is hole-free. The K-level NA combined with the proposed VSPA concept still holds the above properties. Suppose that the moving trail has the same structure as the original NA. According to Proposition 1, the DcA of VSPA-NA-NA is completely consecutive, i.e.,

$$\begin{aligned}&\mathbb{D}_{\text{VSPA-NA-NA}}\\&= \mathbb{U}_{\text{VSPA-NA-NA}}\\&= \{(x,y)\,|\,x,y \in [-N_2(N_1+1):1:N_2(N_1+1)]\}.\end{aligned} \tag{22}$$

In other words, the entire virtual aperture can be used and the DOF of VSPA-NA-NA is equal to its uDOF, i.e.,

$$\begin{aligned}\mathcal{A}_{\text{VSPA-NA-NA}} &= 2(N_2(N_1+1)-1)\times 2(N_2(N_1+1)-1),\\ \mathcal{D}_{\text{VSPA-NA-NA}} &= \mathcal{U}_{\text{VSPA-NA-NA}}\\ &= (2N_2(N_1+1)-1)\times(2N_2(N_1+1)-1).\end{aligned} \tag{23}$$

The optimum parameters to maximize the uDOF are $N_1 = \lfloor \frac{N_s}{2} \rfloor, N_2 = \lceil \frac{N_s}{2} \rceil$.

Although VSPA-NA-NA can reach higher DOF than VSPA-CA-CA with the same $N_s$, it suffers more severe mutual coupling effect because of the dense part in the original NA. Moreover, it consumes more time to complete the motion and sampling since the moving trail in this case is longer than that of VSPA-CA-CA.

Fig. 5 shows an example of VSPA-NA-NA for $N_1 = N_2 = 3$. Fig. 5(a) and 5(b) illustrate the physical geometry and the corresponding DcA, respectively. It can be seen that the hole-free DcA of VSPA-NA-NA reaches high uDOF of $\mathcal{D}_{\text{VSPA-NA-NA}} = 23 \times 23$ with the same number of physical sensors $N_s = N_1 + N_2 = 6$.

### C. VSPA-CA-NA/VSPA-NA-CA

From the above two examples, we can figure out that given the original linear array and the moving trail, the VSPA is easy to construct with few physical sensors. Different combinations of the original linear array and the moving trail can result in different DcAs. Take VSPA-CA-NA and VSPA-NA-CA as examples for comparison. The holes locate in their DcAs can be expressed as

$$\begin{aligned}\mathbb{H}_{\text{VSPA-CA-NA}} = \{(x,y)\,|\,&x = \pm(aM+bN),\\ &y \in [-N_2(N_1+1):1:N_2(N_1+1)]\},\end{aligned}$$

$$\begin{aligned}\mathbb{H}_{\text{VSPA-NA-CA}} = \{(x,y)\,|\,&x \in [-N_2(N_1+1):1:N_2(N_1+1)],\\ &y = \pm(aM+bN)\}.\end{aligned} \tag{24}$$

where $a \geq 0, b > 0, 0 < aM + bN < M(N-1)$. And the AVP and uDOF for each array are

$$\begin{aligned}\mathcal{A}_{\text{VSPA-CA-NA}} &= 2M(N-1)\times 2(N_2(N_1+1)-1),\\ \mathcal{U}_{\text{VSPA-CA-NA}} &= (2M+2N-1)\times(2N_2(N_1+1)-1),\end{aligned} \tag{25}$$

and

$$\begin{aligned}\mathcal{A}_{\text{VSPA-NA-CA}} &= 2(N_2(N_1+1)-1)\times 2M(N-1),\\ \mathcal{U}_{\text{VSPA-NA-CA}} &= (2N_2(N_1+1)-1)\times(2M+2N-1).\end{aligned} \tag{26}$$

It can be figured out that both the physical sensor positions and the DcAs of the two structures are different. The VSPA-CA-NA is physically sparser while the moving distance of VSPA-NA-CA is shorter. But the largest number of consecutive sensors in the DcAs are the same. This fact reminds us that when designing a VSPA-based structure for determined aperture or uDOF, one should make a trade-off between the sensor distribution and the moving distance, in consideration of the physical aperture, the DOF, the mutual coupling, the time consumption etc.

In Fig. 6, a VSPA-CA-NA and a VSPA-NA-CA as well as their DcAs are shown. The array parameters are $M = 3$, $N = 4, N_1 = N_2 = 3$ for both arrays, and the total number of physical sensors is $N_s = M + N - 1 = N_1 + N_2 = 6$. The geometries of the synthetic arrays are different but both of the largest numbers of consecutive sensors are 437. The uDOFs of the two arrays are $\mathcal{U}_{\text{VSPA-CA-NA}} = 19 \times 23$ and $\mathcal{U}_{\text{VSPA-NA-CA}} = 23 \times 19$.

### D. VSPA-MRA-MRA

For generality, we also consider the combination of VSPA and MRA to maximize the achievable uDOF. Table. 1 lists some of the searching results of MRA. It can be seen that when $N_s = 6$, the 1D MRA can generate a hole-free DcA with $\mathcal{U}_{\text{MRA}} = 27$. Thus, the VSPA-MRA-MRA based on this original MRA can reach $\mathcal{U}_{\text{VSPA-MRA-MRA}} = 27 \times 27$, which is higher than that of all the structures mentioned above.

***Remarks:*** Although the geometry of VSPA-NA-NA (or VSPA-CA-CA) may seem like 2D-NA (or 2D-CA) when

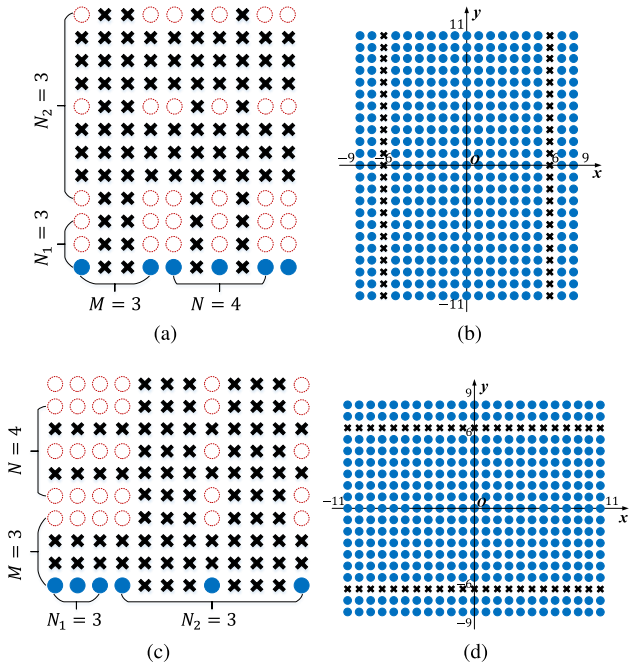


**FIGURE 6.** $M = 3, N = 4, N_1 = N_2 = 3$. (a) The VSPA-CA-NA. (b) The DcA of VSPA-CA-NA. (c) The VSPA-NA-CA. (d) The DcA of VSPA-NA-CA.

**TABLE 1.** Searching results of MRA.

| $\mathbf{N_s}$ | Sensor Position | uDOF |
|---|---|---|
| 3 | $[0, 1, 3]$ | 7 |
| 6 | $[0, 1, 6, 9, 11, 13]$ | 27 |
| 11 | $[0, 1, 3, 6, 13, 20, 27, 34, 38, 42, 43]$ | 87 |
| 12 | $[0, 1, 3, 6, 13, 20, 27, 34, 41, 45, 49, 50]$ | 101 |

**TABLE 2.** Achievable uDOFs comparison of different arrays.

| Arrays | $\mathbf{N_s = 12}$ |
|---|---|
| 2D-CA | $M = 2, N = 3, \mathcal{U} = 6 \times 6$ |
| 2D-NA | $N_1 = 2, N_2 = N_3 = 3, \mathcal{U} = 6 \times 6$ |
| HOBA-2 | $N_x = 6, N_y = 4, \mathcal{U} = 11 \times 7$ |
| LdA | $N_x = 6, N_y = 4, \mathcal{U} = 11 \times 7$ |
| VSPA-CA-CA | $M = 6, N = 7, \mathcal{U} = 25 \times 25$ |
| VSPA-NA-NA | $N_1 = N_2 = 6, \mathcal{U} = 83 \times 83$ |
| VSPA-CA-NA | $M = 6, N = 7, N_1 = N_2 = 6, \mathcal{U} = 25 \times 83$ |
| VSPA-MRA-MRA | $[0, 1, 3, 6, 13, 20, 27, 34, 41, 45, 49, 50]$, $\mathcal{U} = 101 \times 101$ |

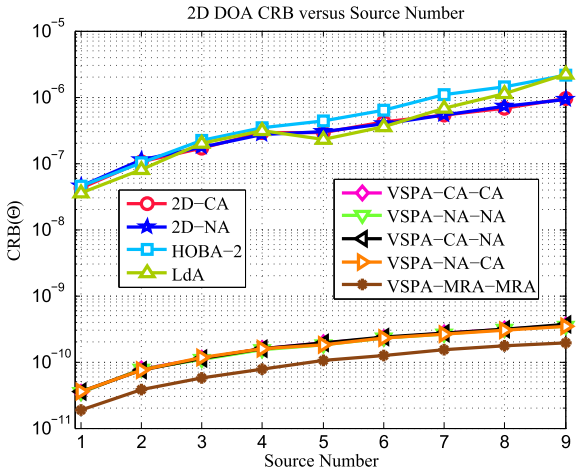


**FIGURE 7.** CRB vs. $Q$ for different structures where SNR is 10dB and $K_s = 1000$.

the parameters are similar, the fact is that they are totally different. Sensor positions of VSPA are determined by the chosen original linear array and moving trail, while that of SPAs follow specific closed-form expressions. The main contribution of VSPA lies on the construction of 2D arrays with only one 1D arrays used. Thus, for the same aperture, VSPA needs less physical sensors. With the same number of sensors, VSPA can reach much higher DOF. As the original linear array and the moving trail can be arbitrarily chosen, VSPA has high flexibility and can be customized to meet different demands. However, VSPA is more time-consuming and stricter to the signal environment.

### *E. ACHIEVABLE uDOF*

In Table. 2, the parameters for different planar arrays and the achievable uDOFs of them are presented for $N_s = 12$. Besides the 2D-CA and 2D-NA mentioned in Section II, two more recently proposed planar arrays are also taken into account, namely the half open box array with two layers (HOBA-2) [34] and the ladder array (LdA) [35]. Both of the two structure are improvements of the open box array (OBA) [36]. The OBA can use $N_s = N_x + 2N_y - 2$ sensors to generate a hole-free DcA with the uDOF of $\mathcal{U}_{\text{OBA}} = (2N_x - 1) \times (2N_y - 1)$. HOBA-2 and LdA can generate the same URA in DcA as their base OBA. From Table. 2 it is clear that when the total number of physical sensors is the same, the uDOFs of VSPA-based arrays are much higher than that of the other planar arrays. And with such high uDOF, more sources can be detected and higher performance of 2D DOA estimation can be achieved.

### *F. Cramér–Rao BOUND*

The Cramér–Rao bound (CRB) offers a lower bound on the variances of unbiased estimates of parameters, which in our case refer to the 2D DOAs. In the following, we derive the 2D DOA CRB expression for VSPA according to [37]. Under the unconditional model assumption (UMA) [38] and further assuming that the sources are known a priori to be uncorrelated, the CRB for coarray-based DOA estimators can be derived.

Recall from (15) and (16) that we have obtained the covariance matrix of the synthetic receiving data, $\mathbf{R}_y$, as well as its vectorized form, $\mathbf{z}$. Define $\boldsymbol{\zeta}$ as the $3Q \times 1$ unknown parameter vector:

$$\boldsymbol{\zeta} = [\boldsymbol{\Theta}^T,\ \tilde{\mathbf{p}}^T,\ \sigma_n^2]^T, \tag{27}$$

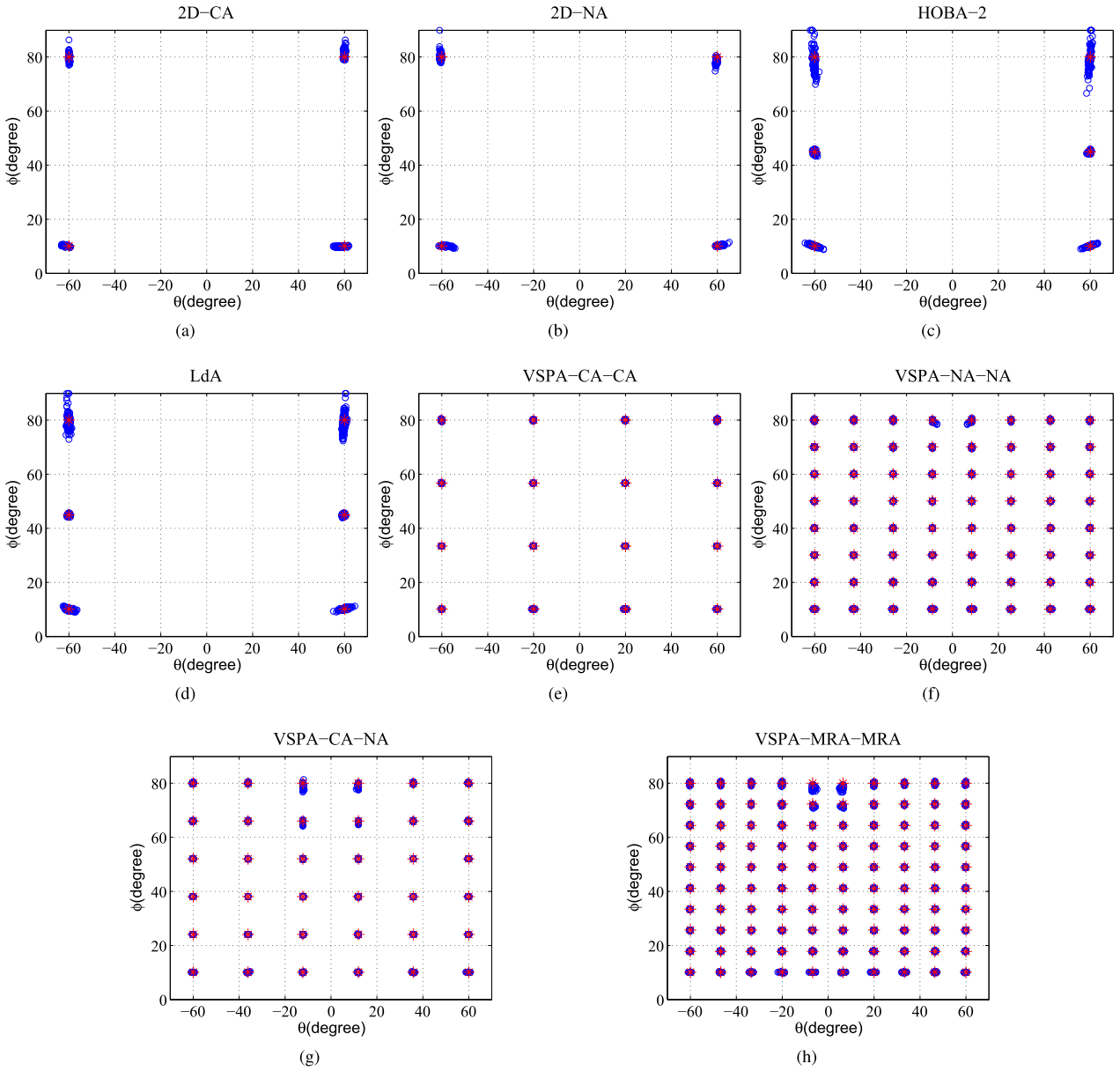


**FIGURE 8.** DOA estimation results for different $N_s = 12$ arrays using SS-UESPRIT. (a) 2D-CA with $M = 2, N = 3$ for $Q = 4$. (b) 2D-NA with $N_1 = 2, N_2 = N_3 = 3$ for $Q = 4$. (c) HOBA-2 with $N_x = 6, N_y = 4$ for $Q = 6$. (d) LdA with $N_x = 6, N_y = 4$ for $Q = 6$. (e) VSPA-CA-CA with $M = 6, N = 7$ for $Q = 20$. (f) VSPA-NA-NA with $N_1 = N_2 = 6$ for $Q = 64$. (g) VSPA-CA-NA with $M = 6, N = 7, N_1 = N_2 = 6$ for $Q = 36$. (h) VSPA-MRA-MRA for $Q = 100$.

where $\boldsymbol{\Theta} = [\cos(\alpha_1), \ldots, \cos(\alpha_Q), \cos(\beta_1), \ldots, \cos(\beta_Q)]^T$ is the vector of the normalized 2D DOAs, and $\tilde{\mathbf{p}}$ is the vector of source power defined in (16). Then, the Fisher Information Matrix (FIM) is given by

$$\begin{aligned}\mathbf{F}(\boldsymbol{\zeta}) &= K_s tr\left(\mathbf{R}_y^{-1}\frac{\partial \mathbf{R}_y}{\partial \boldsymbol{\zeta}}\mathbf{R}_y^{-1}\frac{\partial \mathbf{R}_y}{\partial \boldsymbol{\zeta}}\right)\\ &= K_s\left[vec\left(\frac{\partial \mathbf{R}_y}{\partial \boldsymbol{\zeta}}\right)\right]^H\left(\mathbf{R}_y^{-T}\otimes\mathbf{R}_y^{-1}\right)vec\left(\frac{\partial \mathbf{R}_y}{\partial \boldsymbol{\zeta}}\right)\\ &= K_s\left[\left(\mathbf{R}_y^T\otimes\mathbf{R}_y\right)^{-\frac{1}{2}}\frac{\partial \mathbf{z}}{\partial \boldsymbol{\zeta}}\right]^H\left[\left(\mathbf{R}_y^T\otimes\mathbf{R}_y\right)^{-\frac{1}{2}}\frac{\partial \mathbf{z}}{\partial \boldsymbol{\zeta}}\right],\end{aligned} \tag{28}$$

where the partial derivation $\partial\mathbf{z}/\partial\boldsymbol{\zeta}$ is given by

$$\begin{aligned}\frac{\partial \mathbf{z}}{\partial \boldsymbol{\zeta}} &= \left[\frac{\partial \mathbf{z}}{\partial \boldsymbol{\Theta}}, \frac{\partial \mathbf{z}}{\partial \tilde{\mathbf{p}}}, \frac{\partial \mathbf{z}}{\partial \sigma_n^2}\right]\\ &= \left[\frac{\partial(\mathbf{C}^*\odot\mathbf{C})}{\partial\boldsymbol{\Theta}}\mathbf{R}_s,\ \mathbf{C}^*\odot\mathbf{C},\ \mathbf{i}\right].\end{aligned} \tag{29}$$

Let

$$\begin{aligned}\mathbf{M}_{\boldsymbol{\Theta}} &= \left(\mathbf{R}_y^T\otimes\mathbf{R}_y\right)^{-\frac{1}{2}}\frac{\partial \mathbf{z}}{\partial \boldsymbol{\Theta}},\\ \mathbf{M}_{\boldsymbol{\Delta}} &= \left(\mathbf{R}_y^T\otimes\mathbf{R}_y\right)^{-\frac{1}{2}}\left[\frac{\partial \mathbf{z}}{\partial \tilde{\mathbf{p}}}, \frac{\partial \mathbf{z}}{\partial \sigma_n^2}\right],\end{aligned} \tag{30}$$

then (28) can be expressed as

$$\mathbf{F}(\boldsymbol{\zeta}) = K_s \begin{bmatrix} \mathbf{M}_{\boldsymbol{\Theta}}^H \mathbf{M}_{\boldsymbol{\Theta}} & \mathbf{M}_{\boldsymbol{\Theta}}^H \mathbf{M}_{\boldsymbol{\Delta}} \\ \mathbf{M}_{\boldsymbol{\Delta}}^H \mathbf{M}_{\boldsymbol{\Theta}} & \mathbf{M}_{\boldsymbol{\Delta}}^H \mathbf{M}_{\boldsymbol{\Delta}}. \end{bmatrix} \tag{31}$$

Consequently, the CRB of 2D DOAs can be obtained by the block-wise inversion:

$$\mathrm{CRB}(\boldsymbol{\Theta}) = \frac{1}{K_s} \left[ \mathbf{M}_{\boldsymbol{\Theta}}^H \boldsymbol{\Pi}_{\mathbf{M}_{\boldsymbol{\Delta}}}^{\perp} \mathbf{M}_{\boldsymbol{\Theta}} \right], \tag{32}$$

where $\boldsymbol{\Pi}_{\mathbf{M}_{\boldsymbol{\Delta}}}^{\perp} = \mathbf{I} - \mathbf{M}_{\boldsymbol{\Delta}} \left( \mathbf{M}_{\boldsymbol{\Delta}}{}^H \mathbf{M}_{\boldsymbol{\Delta}} \right)^{-1} \mathbf{M}_{\boldsymbol{\Delta}}$.

In Fig. 7 we examine the dependence of CRB($\boldsymbol{\Theta}$) on the source number $Q$ for 2D-CA, 2D-NA, HOBA-2, LdA and the VSPA-based structures mentioned earlier in this section. For all arrays, the total number of sensors is $N_s = 12$ (see Table 2), the signal-to-noise ratio (SNR) is 10dB, and the number of snapshots is $K_s = 1000$. First of all, it can be seen that all the VSPA-based structures have much lower CRBs than other planar arrays. This can sufficiently validate the effectiveness of our proposed method in 2D DOA estimation. Furthermore, the VSPA-MRA-MRA has the lowest CRB among the VSPA-based structures, since the uDOF of it is the highest.

## V. SIMULATION RESULTS

In this section, we present some simulations to validate the superiority of the proposed VSPA geometry. All the DOA estimation results are through $N_m = 100$ times of independent Monte Carlo trials among 8 array structures, namely 2D-CA, 2D-NA, HOBA-2, LdA, VSPA-CA-CA, VSPA-NA-NA, VSPA-CA-NA and VSPA-MRA-MRA. For fair comparison, the total number of physical sensors for all arrays is set to be $N_s = 12$, and the detailed array parameters can be found in Table. 2. For all arrays, the 2D DOA estimation method is chosen to be the 2D unitary ESPRIT with spatial smoothing.

### A. DETECTABLE NUMBER OF SOURCES

In the first simulation, we examine the number of detectable sources for each array. In all cases, the input SNR is 10dB and $K_s = 1000$. The true 2D DOAs of the $Q$ sources are set to be uniformly distributed in the range $\{(\theta, \phi) \,|\, \theta \in [-60°, 60°], \phi \in [10°, 80°]\}$.

Fig. 8 illustrates the 2D DOA estimation results of all trials. 2D-CA and 2D-NA get similar results of detecting merely $Q = 4$ sources as shown in Fig. 8(a) and Fig. 8(b), since both of their uDOFs are only $6 \times 6$. Obvious errors start to appear when $Q$ gets larger than 6 for them. In Fig. 8(c) and Fig. 8(d), although HOBA-2 and LdA can reach the uDOF of $11 \times 7$, $Q = 6$ sources are almost the extreme for them to distinguish. Especially when the elevation angle $\phi$ is close to 0° or 90°, the estimation accuracy gets obviously worse. However, for the VSPA-based structures in Fig. 8(e)-(h), the estimation results keep precise even when $Q$ is much larger than $N_s$. Especially for VSPA-NA-NA and VSPA-MRA-MRA, up to 64 and 100 distinct sources are detected with little bias. In consequence, for the same $Q$, the VSPA-based structures perform outstandingly over typical SPAs in both number of detectable sources and detection accuracy. This result mainly owes to the fact that the VSPA-based structures can reach sufficiently high uDOF.

### B. DOA ESTIMATION PERFORMANCE

In this simulation, we examine the *Root Mean-Square Error (RMSE)* of different array structures through all trials for DOA estimation performance comparison. The RMSE is expressed as

$$\mathrm{RMSE} = \sqrt{\frac{1}{QN_m} \sum_{n=1}^{N_m} \sum_{q=1}^{Q} \left(\hat{\theta}_q(n) - \theta_q\right)^2 + \left(\hat{\phi}_q(n) - \phi_q\right)^2}, \tag{33}$$

where $(\hat{\theta}_q(n), \hat{\phi}_q(n))$ is the estimated 2D DOA of $(\theta_q, \phi_q)$ for the $n$th Monte Carlo trial.

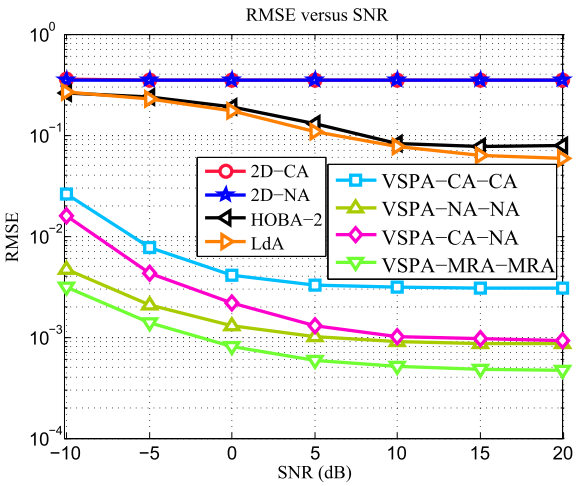


**FIGURE 9.** RMSE vs. SNR for different arrays where $K_s = 1000$ and $Q = 9$.

In Fig. 9, the dependence of RMSE on the input SNR varying from −10dB to 20dB is examined. The number of sources is $Q = 9$ and the number of physical sensors is $N_s = 12$ for all arrays. $K_s = 1000$ snapshots are taken in each measurement. It can be seen that neither of the 2D-CA and the 2D-NA has sufficient ability to detect $Q = 9$ sources, since both of their uDOFs are $6 \times 6$ and even lower after 2D spatial smoothing. The performances of HOBA-2 and LdA are better than 2D-CA and 2D-NA, but the RMSEs saturate to a relatively high level as SNR increases. As for the VSPA-based structures, all of them get much more accurate results than the previous arrays. VSPA-MRA-MRA performs the best, followed by VSPA-NA-NA, then VSPA-CA-NA, and finally VSPA-CA-CA. The results completely match the uDOFs of these structures.

Fig. 10 illustrates the RMSEs for different number of snapshots, which varies from 200 to 6000. The SNR is 10dB in all cases. Similar to the last experiment, both of the 2D-CA and the 2D-NA fail to accomplish the estimations with $N_s = 12$. Errors for HOBA-2 and LdA reduce to an acceptable amount

when $K_s$ is sufficiently large. The VSPA-based structures keep performing well throughout all cases, even when $K_s$ is only 200. The order of their performance still obeys the order of their uDOFs. This simulation along with the last one about SNR can verify that the proposed VSPA is effective in enhancing the performance of 2D DOA estimation.

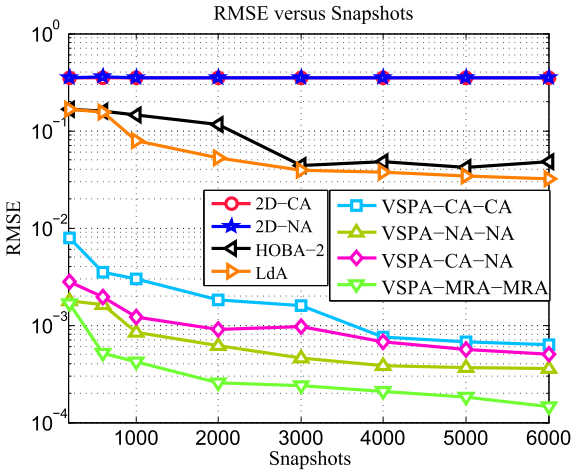


**FIGURE 10.** RMSE vs. number of snapshots for different arrays where SNR is 10dB and $Q = 9$.

In the above two experiments, the SPAs in previous works perform not well since the uDOFs of them are not enough. Thus, in the next simulation we present the RMSE for different $Q$ as shown in Fig. 11. Note that $N_s = 12$, SNR is 10dB and $K_s = 1000$ for all arrays in all cases. $Q$ is set to vary from 1 to 9 because UESPRIT fails to give resolutions to 2D-CA and 2D-NA for larger $Q$. The result shows that 2D-CA and 2D-NA start to make obvious errors when $Q > 4$, which is identical to the previous two simulations. The RMSEs of HOBA-2 and LdA gradually rise as the source number grows. However, the VSPA-based structures keep high performance for all cases as the uDOFs of them are much larger than 9. This result accords with the calculated CRBs in Fig. 7.

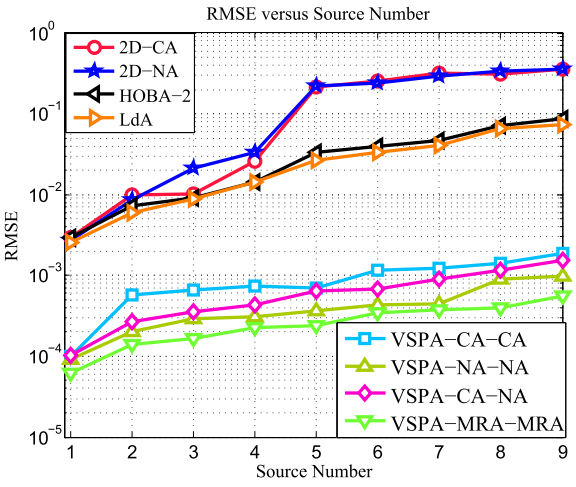


**FIGURE 11.** RMSE vs. source number for different arrays where SNR is 10dB and $K_s = 1000$.

Consequently, all simulations above verify the superiority of the proposed VSPA geometry. When designing VSPAs, the choice of original linear array mainly affects the distribution of physical sensors, while the choice of moving trail mainly determines the final 2D aperture and brings in the complexity of sampling.

## VI. CONCLUSION

In this paper, we utilize the thought of synthetic aperture processing to make an arbitrary linear array move vertically to generate a synthetic planar array, i.e., VSPA geometry. The VSPA is easy to construct and has high flexibility to design for specific requirements. The sparsity of array geometry and high DOF can be satisfied at the same time for proper choice of the original linear array and the moving trail. Simulation results have validated the superiority of the VSPA-based arrays over typical 2D arrays when the number of physical sensors are the same. The enhanced performance of VSPA is at cost of extra time consumption. Thus, in practice the moving distance and velocity should always be taken into consideration to hold the assumption of stationary signal environment.

## REFERENCES

[1] J. Li and P. Stoica, *MIMO Radar Signal Processing*. Hoboken, NJ, USA: Wiley, 2008.
[2] H. Krim and M. Viberg, "Two decades of array signal processing research: The parametric approach," *IEEE Signal Process. Mag.*, vol. 13, no. 4, pp. 67–94, Jul. 1996.
[3] P. Stoica, Z. Wang, and J. Li, "Extended derivations of MUSIC in the presence of steering vector errors," *IEEE Trans. Signal Process.*, vol. 53, no. 3, pp. 1209–1211, Mar. 2005.
[4] H. L. Van Trees, *Optimum Array Processing: Part IV of Detection, Estimation, and Modulation Theory*. Hoboken, NJ, USA: Wiley, 2004.
[5] R. T. Hoctor and S. A. Kassam, "The unifying role of the coarray in aperture synthesis for coherent and incoherent imaging," *Proc. IEEE*, vol. 78, no. 4, pp. 735–752, Apr. 1990.
[6] A. Moffet, "Minimum-redundancy linear arrays," *IEEE Trans. Antennas Propag.*, vol. AP-16, no. 2, pp. 172–175, Mar. 1968.
[7] E. Vertatschitsch and S. Haykin, "Nonredundant arrays," *Proc. IEEE*, vol. 74, no. 1, p. 217, Jan. 1986.
[8] P. Pal and P. P. Vaidyanathan, "Nested arrays: A novel approach to array processing with enhanced degrees of freedom," *IEEE Trans. Signal Process.*, vol. 58, no. 8, pp. 4167–4181, Aug. 2010.
[9] P. Pal and P. P. Vaidyanathan, "Coprime sampling and the music algorithm," in *Proc. Digit. Signal Process. Signal Process. Educ. Meeting (DSP/SPE)*, Jan. 2011, pp. 289–294.
[10] C.-L. Liu and P. P. Vaidyanathan, "Super nested arrays: Linear sparse arrays with reduced mutual coupling—Part I: Fundamentals," *IEEE Trans. Signal Process.*, vol. 64, no. 15, pp. 3997–4012, Aug. 2016.
[11] C.-L. Liu and P. P. Vaidyanathan, "Super nested arrays: Linear sparse arrays with reduced mutual coupling—Part II: High-order extensions," *IEEE Trans. Signal Process.*, vol. 64, no. 16, pp. 4203–4217, Aug. 2016.
[12] J. Liu, Y. Zhang, Y. Lu, S. Ren, and S. Cao, "Augmented nested arrays with enhanced DOF and reduced mutual coupling," *IEEE Trans. Signal Process.*, vol. 65, no. 21, pp. 5549–5563, Nov. 2017.
[13] S. Qin, Y. D. Zhang, and M. G. Amin, "Generalized coprime array configurations for direction-of-arrival estimation," *IEEE Trans. Signal Process.*, vol. 63, no. 6, pp. 1377–1390, Mar. 2015.
[14] X. Wang, Z. Chen, S. Ren, and S. Cao, "DOA estimation based on the difference and sum coarray for coprime arrays," *Digit. Signal Process.*, vol. 69, pp. 22–31, Oct. 2017.
[15] Z. Chen, Y. Ding, S. Ren, and Z. Chen, "A novel nested configuration based on the difference and sum co-array concept," *Sensors*, vol. 18, no. 9, p. 2988, Sep. 2018.

[16] N.-C. Yen and W. Carey, "Application of synthetic-aperture processing to towed-array data," *J. Acoust. Soc. Amer.*, vol. 86, no. 2, pp. 754–765, 1989.
[17] R. Williams and B. Harris, "Passive acoustic synthetic aperture processing techniques," *IEEE J. Ocean. Eng.*, vol. 17, no. 1, pp. 8–15, Jan. 1992.
[18] S. Stergiopoulos and H. Urban, "A new passive synthetic aperture technique for towed arrays," *IEEE J. Ocean. Eng.*, vol. 17, no. 1, pp. 16–25, Jan. 1992.
[19] J. Ramirez and J. L. Krolik, "Synthetic aperture processing for passive co-prime linear sensor arrays," *Digit. Signal Process.*, vol. 61, pp. 62–75, Feb. 2017.
[20] G. Qin, Y. D. Zhang, and M. G. Amin, "DOA estimation exploiting moving dilated nested arrays," *IEEE Signal Process. Lett.*, vol. 26, no. 3, pp. 490–494, Mar. 2019.
[21] G. Qin, M. G. Amin, and Y. D. Zhang, "DOA estimation exploiting sparse array motions," *IEEE Trans. Signal Process.*, vol. 67, no. 11, pp. 3013–3027, Jun. 2019.
[22] T. C. Yang, "Measurements of temporal coherence of sound transmissions through shallow water," *J. Acoust. Soc. Amer.*, vol. 120, no. 5, pp. 2595–2614, Nov. 2006.
[23] Y. Zhou, Y. Li, and C. Wen, "The multi-level dilated nested array for direction of arrival estimation," *IEEE Access*, vol. 8, pp. 43134–43144, 2020.
[24] S. Li and X.-P. Zhang, "A new approach to construct virtual array with increased degrees of freedom for moving sparse arrays," *IEEE Signal Process. Lett.*, vol. 27, pp. 805–809, 2020.
[25] Z. Shi, X. Zhang, and L. Xu, "DOA estimation of multiple sources for a moving array in the presence of phase noise," *IET Signal Process.*, vol. 13, no. 1, pp. 29–35, Feb. 2019.
[26] P. Pal and P. Vaidyanathan, "Nested arrays in two dimensions, part I: Geometrical considerations," *IEEE Trans. Signal Process.*, vol. 60, no. 9, p. 4694, Jun. 2012.
[27] P. Pal and P. P. Vaidyanathan, "Nested arrays in two dimensions, part II: Application in two dimensional array processing," *IEEE Trans. Signal Process.*, vol. 60, no. 9, pp. 4706–4718, Sep. 2012.
[28] P. P. Vaidyanathan and P. Pal, "Sparse coprime sensing with multidimensional lattice arrays," in *Proc. Digit. Signal Process. Signal Process. Educ. Meeting (DSP/SPE)*, Jan. 2011, pp. 425–430.
[29] P. P. Vaidyanathan and P. Pal, "Theory of sparse coprime sensing in multiple dimensions," *IEEE Trans. Signal Process.*, vol. 59, no. 8, pp. 3592–3608, Aug. 2011.
[30] S. Stergiopoulos and E. J. Sullivan, "Extended towed array processing by an overlap correlator," *J. Acoust. Soc. Amer.*, vol. 86, no. 1, pp. 158–171, Jul. 1989.
[31] C.-L. Liu and P. P. Vaidyanathan, "Remarks on the spatial smoothing step in coarray MUSIC," *IEEE Signal Process. Lett.*, vol. 22, no. 9, pp. 1438–1442, Sep. 2015.
[32] M. D. Zoltowski, M. Haardt, and C. P. Mathews, "Closed-form 2-D angle estimation with rectangular arrays in element space or beamspace via unitary ESPRIT," *IEEE Trans. Signal Process.*, vol. 44, no. 2, pp. 316–328, 1996.
[33] S. Ren, X. Ma, S. Yan, and C. Hao, "2-D unitary ESPRIT-like direction-of-arrival (DOA) estimation for coherent signals with a uniform rectangular array," *Sensors*, vol. 13, no. 4, pp. 4272–4288, Mar. 2013.
[34] C.-L. Liu and P. P. Vaidyanathan, "Hourglass arrays and other novel 2-D sparse arrays with reduced mutual coupling," *IEEE Trans. Signal Process.*, vol. 65, no. 13, pp. 3369–3383, Jul. 2017.
[35] S. Ren, X. Li, X. Luo, and W. Wang, "Extensions of open box array with reduced mutual coupling," *IEEE Sensors J.*, vol. 18, no. 13, pp. 5475–5484, Jul. 2018.
[36] C. R. Greene and R. C. Wood, "Sparse array performance," *J. Acoust. Soc. Amer.*, vol. 63, no. 6, pp. 1866–1872, 1978.
[37] C.-L. Liu and P. P. Vaidyanathan, "Cramér–Rao bounds for coprime and other sparse arrays, which find more sources than sensors," *Digit. Signal Process.*, vol. 61, pp. 43–61, Feb. 2017.
[38] P. Stoica and A. Nehorai, "Performance study of conditional and unconditional direction-of-arrival estimation," *IEEE Trans. Acoust., Speech, Signal Process.*, vol. 38, no. 10, pp. 1783–1795, Oct. 1990.

**GUIYU WANG** was born in Sichuan, China, in January 1991. He received the B.Eng. degree in information countermeasures from the Beijing Institute of Technology, Beijing, China, in 2013, where he is currently pursuing the Ph.D. degree in information and communication Engineering. His research interests include sparse array processing, direction-of-arrival estimation, and signal processing.

**ZESONG FEI** (Senior Member, IEEE) received the Ph.D. degree in electronic engineering from the Beijing Institute of Technology (BIT) in 2004. He is currently a Professor with the Research Institute of Communication Technology (RICT), BIT, where he is involved in the design of the next-generation high-speed wireless communication systems. His research interests include wireless communications and multimedia signal processing. He is a Principal Investigator of projects funded by the National Natural Science Foundation of China. He is also a Senior Member of the Chinese Institute of Electronics and the China Institute of Communications.

**SHIWEI REN** received the B.Eng. degree in information engineering from the Beijing Institute of Technology, Beijing, China, in 2008, and the Ph.D. degree in signal and information processing from the University of Chinese Academy of Sciences, Beijing, in 2013. In 2013, she joined the Faculty of the School of Information and Electronics, Beijing Institute of Technology. Her current research interests include direction-of-arrival estimation, sparse array design, and array signal processing.